Molecular Immunology 114 (2019) 30–40

Contents lists available at ScienceDirect

Molecular Immunology

journal homepage: www.elsevier.com/locate/molimm

Identification of a distinct subset of disease-associated gain-of-function missense mutations in the STAT1 coiled-coil domain as system mutants

Jana Petersen[a], Julia Staab[a], Oliver Bader[b], Timo Buhl[c], Aleksandar Ivetic[d], Thomas Meyer[a,*]

[a] Department of Psychosomatic Medicine and Psychotherapy, University Medical Center Göttingen, Göttingen, Germany
[b] Institute of Medical Microbiology, University Medical Center Göttingen, Göttingen, Germany
[c] Department of Dermatology, Venereology and Allergology, University Medical Center Göttingen, Göttingen, Germany
[d] School of Cardiovascular Medicine and Sciences, James Black Centre, BHF Centre of Research Excellence, King's College London, London, UK

ARTICLE INFO

Keywords:
STAT1
Interferon signalling
Dimerization
Gain-of-function mutation
Chronic mucocutaneous candidiasis

ABSTRACT

Heterozygous gain-of-function (GOF) mutations in the cytokine-regulated transcription factor STAT1 (signal transducer and activator of transcription 1) lead to chronic mucocutaneous candidiasis (CMC). However, the molecular basis of these pathogenic missense mutations is largely unknown. In this study, we characterized in more detail the CMC-associated GOF substitution mutation of arginine-to-tryptophan at position 274 (R274W) and, in addition, the adjacent glutamine-to-alanine mutation at position 275 (Q275A). Both mutants displayed elevated tyrosine phosphorylation levels, prolonged nuclear accumulation, and increased transcriptional responses to interferon-γ (IFNγ) stimulation. No difference was observed between wild-type (WT) and mutant STAT1 in DNA sequence-specificity or dissociation kinetics from high-affinity DNA-binding elements known as gamma-activated sites (GAS). Furthermore, all variants exhibited similar cooperative DNA binding. Unexpectedly, *in vitro* dephosphorylation rates using the recombinant STAT1-inactivating Tc45 phosphatase in both the absence and presence of double-stranded GAS elements were similar in all STAT1 variants. Likewise, the rate of tyrosine phosphorylation by Janus kinase 2 (JAK2) was unaltered as compared to the WT molecule, excluding that the phenotype of these mutants is caused by either defective Tc45-catalyzed dephosphorylation or JAK2-induced hyper-activation. Interestingly, within 10 min of IFNγ exposure, the majority of R274W and Q275A molecules had entered the nucleus, whereas the wild-type protein remained predominantly cytosolic. Thus, the exchange of critical residues located at the binding interface in the antiparallel dimer conformer led to a premature accumulation of phospho-STAT1 in the nuclear compartment. In summary, our data show that the hyper-activity of the GOF mutations results, at least in part, from the premature nuclear import of the tyrosine-phosphorylated molecules and not from alterations in their phosphorylation or dephosphorylation rates.

1. Introduction

Signal transducer and activator of transcription 1 (STAT1), the founding member of the family of STAT proteins, plays an important role as interferon-driven transcription factor in the regulation of immune responses. Ligand binding of interferon-γ (IFNγ) to its membrane receptor induces the dimerization of the receptor subunits which is followed by the auto-phosphorylation of Janus kinases (JAKs), which are non-covalently associated to the receptor (Levy and Darnell, 2002). Activated JAKs then phosphorylate the intracellular receptor domains, creating phospho-tyrosine docking sites for the recruitment of STAT1 molecules. STAT1 proteins are bound *via* their Src-homology-2-(SH2) domain to the phosphorylated sites at the receptor tail and are subsequently phosphorylated by the JAKs on a critical tyrosine residue (Y701) (Shuai et al., 1992). This allows the formation of phospho-STAT1 homodimers in a parallel dimer conformation stabilized through reciprocal SH2-phosphotyrosine interactions between the two protomers (Shuai et al., 1994). The activated STAT1 dimers are then translocated to the nucleus, where they bind to palindromic gamma-activated sites (GAS) in the promoter regions of IFNγ-responsive genes containing the consensus sequence 5´-TTC(N)$_{3-4}$GAA-´3 (Decker et al., 1997). After dissociation from DNA and dephosphorylated by the nuclear tyrosine phosphatase Tc45, STAT1 is exported back to the cytoplasm in order to participate in another round of nucleocytoplasmic shuttling (Haspel and Darnell, 1999; ten Hoeve et al., 2002; Meyer et al., 2003). Beside the parallel dimer conformation required for

* Corresponding author at: Klinik für Psychosomatische Medizin und Psychotherapie, Georg-August-Universität Göttingen, Waldweg 33, 37073 Göttingen, Germany.
E-mail address: thomas.meyer@med.uni-goettingen.de (T. Meyer).

https://doi.org/10.1016/j.molimm.2019.07.008
Received 24 March 2019; Received in revised form 26 June 2019; Accepted 10 July 2019
Available online 20 July 2019

nuclear import and DNA binding of the tyrosine-phosphorylated STAT1, biochemical experiments have demonstrated the presence of an antiparallel dimer conformation (Zhong et al., 2005; Mertens et al., 2006). In the crystal structure of the antiparallel dimer, the two SH2 domains are located at opposite ends of the dimer, while the dimer interface is formed between complementary interactions from the coiled-coil domain of one protomer to the DNA-binding domain of the other, and *vice versa* (Mao et al., 2005).

Given that STAT1 is required for the antimicrobial action of interferons, loss-of-function mutations in the gene encoding STAT1 have been identified which cause susceptibility to a range of infections in human subjects, including severe viral and bacterial infections, such as non-tuberculous mycobacterial disease (Dupuis et al., 2001, 2003). Autosomal dominant gain-of-function (GOF) mutations in the *STAT1* gene result in bacterial infections mostly caused by Staphylococcus aureus, autoimmune manifestations, and chronic mucocutaneous candidiasis (CMC), which is a severe immune dysregulation characterized by recurrent or persistent infections with *Candida albicans* affecting the mucous membranes, skin and nails (Liu et al., 2011; van de Veerdonk et al., 2011; Depner et al., 2016; Toubiana et al., 2016). Besides mutations in the *AIRE* gene (autoimmune regulator), monogenic mutations conferring CMC have been identified in regions of the *STAT1* gene encoding the coiled-coil domain and the DNA-binding domain, which are both engaged in the formation of the antiparallel dimer. Recently, Fujiki and colleagues have shown that, while the CMC-associated pathogenic R274Q mutation resulted in persistent tyrosine phosphorylation and increased transcriptional activity, it did not affect the repertoire of STAT1-regulated target genes at a genome-wide expression level (Fujiki et al., 2017). However, it is unclear whether the destabilization of the antiparallel dimer formation caused by the similar R274W substitution alters the phosphorylation kinetics by JAKs and/or the dephosphorylation by the STAT1-inactivating Tc45 phosphatase. In addition, it is not known whether this substitution mutant in the coiled-coil domain affects nuclear accumulation upon cell stimulation with IFNγ. In the present paper, we have addressed these questions and found that this mutant differs from other STAT1 GOF mutants with regard to the molecular mechanism leading to its hyper-activation.

2. Materials and methods

2.1. Plasmids, mutagenesis and cell culture

Two expression vectors were used for this study: pEGFP-N1-STAT1, termed pSTAT1-GFP, coding for a carboxy-terminal fusion of full-length human STAT1 (amino acids 1–746) with green fluorescent protein (GFP), and pcDNA3.1-STAT1 (pSTAT1, Invitrogen), which coded for untagged, full-length human STAT1 cDNA (Begitt et al., 2000). Point mutations were introduced in the expression vectors by site-directed mutagenesis using the QuikChange II kit from Stratagene, as recommended by the manufacturer. The following primers were used with mutated codons underlined (only forward primers are shown):

R274Wf; 5´-GAGAGTCTGCAGCAAGTTTGGCAGCAGCTTAAAAAGTTG-´3,

Q275Af; 5´-GTCTGCAGCAAGTTCGGGCGCAGCTTAAAAAGTTGGAGG-´3, and

K278Af; 5´-CAAGTTCGGCAGCAGCTTGCAAAGTTGGAGGAATTGGAAC-´3.

All mutations were verified by standard didesoxy-termination DNA sequencing (Seqlab) and the resulting plasmids were used for transfection. HeLa cells and STAT1-negative U3A cells (Müller et al., 1993) were cultured in a humidified 5% CO_2 atmosphere at 37 °C in RPMI 1640 medium (Lonza) and Dulbecco's modified Eagle's medium (PAA Laboratories) supplemented with 10% foetal calf serum (FCS; Biochrom), 1% penicillin, 1% streptomycin, and (only for U3A cells) 0.04 μg/ml puromycin. Cells were transfected with MegaTran1.0 (Origene) and on the next day either left untreated or stimulated with 50 ng/ml of recombinant human IFNγ (Biomol) for the indicated times. Subsequently, cells were incubated with 1 μM of the potent kinase inhibitor staurosporine (Sigma-Aldrich) for the indicated times. Alternatively, reconstituted U3A cells were exposed to IFNα (500 U/ml; Biomol).

2.2. Protein extraction and Western blotting

STAT1-expressing cells grown on 6-well dishes were lysed on ice for 5 min in 50 μl cytoplasmic extraction buffer (20 mM Hepes, pH 7.4, 10 mM KCl, 10% (v/v) glycerol, 1 mM EDTA, 0.1 mM Na_3VO_4, 0.1% IGEPAL-CA-360, 3 mM DTT, 0.4 mM Pefabloc (Sigma-Aldrich), and Complete Mini protease inhibitors (Roche)). The extracts were centrifuged at 16,000 *g* for 15 s at 4 °C. The supernatants were spun again for 5 min at 16,000 *g* and collected as cytoplasmic extracts. The pellets from the first centrifugation step were resuspended in 50 μl nuclear extraction buffer (20 mM Hepes, pH 7.4, 420 mM KCl, 20% (v/v) glycerol, 1 mM EDTA, 0.1 mM Na_3VO_4, 3 mM DTT, 0.4 mM Pefabloc, and Complete Mini protease inhibitors) and left on ice for 30 min. After centrifugation at 16,000 *g* for 15 min and 4 °C, the nuclear extracts were mixed with the same amount of cytoplasmic extracts from the same cells. The combined cellular extracts were boiled for 3 min in SDS sample buffer and resolved by 10% SDS-PAGE with subsequent transfer onto PVDF membranes. The membranes were incubated with a monoclonal phospho-Tyr701-specific STAT1 antibody (Cell Signaling, 58D6) and after extensive washing exposed to a conjugated secondary antibody (LI-COR). To determine the amount of total STAT1 from the same blot, PVDF membranes were stripped off bound immunoreactivity in a buffer containing 2% SDS, 0.7% β-mercaptoethanol, and 62.5 mM Tris-HCl, pH 6.8, for 60 min at 60 °C, and were then reprobed with the polyclonal STAT1-specific antibody E-23 (Santa Cruz Biotechnology). Immunoreactivity was detected using a secondary anti-rabbit IRDye 800CW antibody on a LI-COR Odyssey imaging system.

2.3. In vitro phosphorylation and dephosphorylation assays

The *in vitro* dephosphorylation assay was performed at 30 °C for the indicated times with 10 μl of whole cell extracts from STAT1-reconstituted, IFNγ-pretreated U3A cells by adding a similar volume of phospatase reaction buffer (25 mM Tris-HCl, pH 7.5, 50 mM KCl, 5 mM EDTA, 20 mM dithiothreitol, 0.5 mg/ml bovine serum albumin, 2 U of the T-cell protein tyrosine phosphatase Tc45 (Biomol), and Complete protease inhibitors). In the phosphatase reactions, either no DNA or duplex oligonucleotides containing one or two GAS elements in tandem orientation (termed GAS-nonGAS and 2xGAS, respectively) at a concentration of 25 nM were present. Reactions were stopped by adding SDS sample buffer and boiling the samples for 3 min. Tyrosine-phosphorylated and total STAT1 were probed on the same PVDF membrane by means of Western blotting. For phosphorylation assays, extracts from IFNγ-untreated, STAT1-reconstituted U3A cells were used. The kinase buffer contained 50 mM Hepes, pH 7.4, 3 mM $MgCl_2$, 3 mM $MnCl_2$, 3 μM vanadate, 10 mM DTT, 0.1 mM ATP, and 4 μg/ml of recombinant JAK2 (Enzo Life Science). The *in vitro* phosphorylation reactions were carried out at 30 °C with 10 μl of whole cell extracts for the indicated times.

2.4. Fluorescence techniques

T regulatory cells were detected as $CD3^+$ $CD4^+$ $CD25^{high}CD127^{low}$-positive peripheral blood cells by means of flow cytometry (Seddiki et al., 2006). The kinetics of IFNγ-induced nuclear accumulation of wild-type (WT) and mutant STAT1 was monitored in cells by direct fluorescence microscopy. Transiently transfected HeLa cells expressing GFP-tagged STAT1 were treated as indicated or left untreated. Cells were fixed in 4% paraformaldehyde in phosphate-buffered saline (PBS) for 15 min at room temperature (RT) and subsequently nuclei were

stained for 10 min with 5 μg/ml of Hoechst dye, 33258 (Sigma-Aldrich). Samples were mounted in fluorescence mounting medium (Southern Biotech) and the intracellular GFP localization visualized using an Axiovert 200 M microscope (Carl Zeiss) equipped with appropriate fluorescence filters. Images obtained from a CCD camera were further processed with the Image-Pro Plus 5.1 (Media Cybernetics) software. Fluorescence intensities were determined both in the nucleus and in the cytoplasm.

Cytokine-induced nuclear accumulation of recombinant untagged STAT1 was detected by means of immunocytochemistry. Briefly, U3A cells grown on 8-well chamber slides were reconstituted with recombinant STAT1 and one day after transfection treated with IFNγ for 45 min or left untreated. Cells were exposed to the kinase inhibitor staurosporine (1 μM) for the indicated times and then fixed with methanol at −20 °C for 15 min. After two washes in PBS, cells were permeabilized for 20 min with 1.0% Triton X-100 in PBS. Non-specific binding was blocked by incubation with 25% FCS/PBS for 45 min at RT. Samples were first incubated for 45 min with the anti-STAT1 antibody E-23 (diluted 1:1000 in 25% FCS/PBS) and, after three washes in PBS, for 45 min at RT exposed to a Cy3-conjugated secondary antibody (Dianova, diluted 1:500 in 25% FCS/PBS). Nuclei were stained with Hoechst dye and images captured by fluorescence microscopy. The mean nuclear-to-total cytoplasmic fluorescence intensities including their standard deviations were calculated from 20 randomly selected transfected cells.

2.5. Electrophoretic mobility shift assay

STAT1 variants were probed for DNA-binding activity to various duplex oligonucleotides containing consensus or modified GAS sites by means of electrophoretic mobility shift assays (EMSA). Per reaction, 4 μl of cellular extracts from IFNγ-stimulated cells expressing recombinant STAT1 were incubated with 8 μl of EMSA reaction buffer containing 1 ng of the [^{33}P]-labelled duplex oligonucleotide probe, generated by an end-filling reaction using the Klenow fragment (New England Biolabs). The following duplex oligonucleotides were used (4 bp T overhangs at the 5′ ends and the respective antisense oligos are not included, GAS sites are underlined): M67; 5´-CGACATTTCCCGTAAAT CTG-´3,

2xGAS; 5´-CGTTTCCCCGAAATTGACGGATTTCCCCGAAAC-´3,

GAS-nonGAS; 5´-CGTTTCCCCGAAATTGACGGATTTACCCCAAC-´3, and

2xnonGAS; 5´-CGTTTACCCCAAATTGACGGATTTACCCCAAC-´3.

For competition experiments, cell lysates were incubated with [^{33}P]-labelled duplex oligonucleotides in EMSA reaction buffer for 15 min at RT, and subsequently challenged by a 750-fold molar excess of unlabelled M67 DNA incubated for the indicated times. In supershift assays, 20 ng of either the STAT1-specific antibody E-23 or a non-specific STAT3 antibody were added to the reaction for 40 min at RT. The reactions were loaded on a 4.8% 29:1 acrylamide:bisacrylamide gel at 4 °C and separated at 400 V. DNA-binding activities were visualized on vacuum-dried gels using the laser phosphorimaging system Typhoon FLA 9500 (GE Healthcare Life Sciences).

2.6. Reporter gene assays and real-time PCR

U3A cells grown on 48-well plates were co-transfected in each well with three vectors: a luciferase reporter (70 ng), a constitutively expressed β-galactosidase plasmid (200 ng), and an expression plasmid encoding WT or mutant STAT1 (250 ng). The reporters contained either the 5´-region of the human intercellular adhesion molecule 1 (*ICAM-1*) gene 339 bp relative to the transcription start site (termed pIC-339) or a triple Ly6E STAT-binding site (termed 3xLy6E). One day after transfection, cells were either left untreated or treated for 6 h with IFNγ, before cell extracts were prepared with a lysis buffer containing 25 mM glycylglycine, 1% Triton X-100, 15 mM $MgSO_4$, 4 mM EGTA, 0.4 mM Pefabloc, 3 mM 1,4-dithiothreitol, pH 7.8, and Complete protease inhibitors. Luciferase expression was assessed (Promega) using the luminometer Centro KS LB960 (Berthold Technologies) and normalized to the corresponding β-galactosidase activity, which was measured spectroscopically at 420 nm. The experiment was repeated in triplicate, and six independent transfections were tested for each STAT1 variant and stimulation mode.

For expression of endogenous target genes, U3A cells reconstituted with recombinant, untagged STAT1 were cultured for 15 h in Dulbecco's modified Eagle's medium supplemented with 1% FCS, before they were either left untreated or stimulated for 6 h with IFNγ. RNA was isolated using the peqGold Total RNA kit (Peqlab), and first-strand cDNA synthesis was performed using the Verso cDNA Synthesis kit (Thermo Fisher Scientific). Real-time PCR reactions were carried out in a total volume of 20 μl, containing 25 ng cDNA, 70 nmol/l of each specific primer, and 10 μl of Absolute Blue qPCR SYBR Green Mix (Thermo Fisher Scientific). The following primer pairs were used:

CCL2F; 5´-CCAGTCACCTGCTGTTATAAC-´3,
CCL2R; 5´-TGGAATCCTGAACCCACTTCT-´3,
CXCL10F; 5´-ATTCTGAGCCTACAGCAGAG -´3,
CXCL10R; 5´-GCTTGCAGGAATAATTTCAA -´3,
IFI56KF; 5´-TAGCCAACATGTCCTCACAGAC-´3,
IFI56KR; 5´-TCTTCTACCACTGGTTTCATGC-´3,
IRF1F; 5´-AGCTCAGCTGTGCGAGTGTA-´3,
IRF1R; 5´-TAGCTGCTGTGGTCATCAGG-´3,
GAPDHF; 5´-GAAGGTGAAGGTCGGAGTC-´3,
GAPDHR; 5´-GAAGATGGTGATGGGATTTC-´3,
MIG1F; 5´-CCACCGAGATCCTTATCGAA-´3,
MIG1R; 5´-CTAACCGACTTGGCTGCTTC-´3,
MX1F; 5´-CAATCAGCCTGCTGACATTG-´3,
MX1R; 5´-TGTCTCCTGCCTCTGGATG-´3.
RIGGF; 5´-TTGGCCTACATAAAACACCT´3,
RIGGR; 5´-GAAAATTTCTTGCAGGTTTG-´3,
STAT1F; 5´-CCGTTTTCATGACCTCCTGT-´3, and
STAT1R; 5´-TGAATATTCCCCGACTGAGC-´3.

The PCR protocol run on an Eppendorf cycler included a denaturation step at 95 °C for 15 min and 40 cycles of denaturation at 95 °C for 15 s, annealing at 55 °C for 30 s, and extension at 72 °C for 30 s. After the final amplification step, a melting curve analysis was performed using a temperature gradient from 60 °C to 95 °C in 0.5 °C increment steps and fluorescence being measured at each temperature for a period of 10 s. All reactions were carried out in at least triplicates. The relative expression of a transcript was normalized to the expression of *GAPDH* as determined for each sample. The ΔΔCt-method was used to determine comparative relative expression levels, based on the formula $2^{-(\Delta Ct\ target\ -\ \Delta Ct\ reference\ sample)}$.

2.7. Data analysis

Digital images were processed by ImageJ software. For each STAT1 variant and stimulation mode, means and standard deviations were calculated. Differences between WT and mutant protein were assessed using Student's *t* tests and Mann-Whitney-Wilcoxon tests, where appropriate. Data were analyzed using the Sigmastat (Systat Software) program, and a p value ≤ 0.05 was considered to indicate statistical significance.

3. Results

3.1. Long-term ruxolitinib treatment resulted in continuous amelioration of CMC caused by the R274Q mutation

Previously, we reported that treatment with the potent JAK inhibitor ruxolitinib improved the clinical condition of an adult CMC patient carrying the heterozygous STAT1 GOF mutation R274Q, who was suffering from severe dysphagia due to ulcerative mucositis and

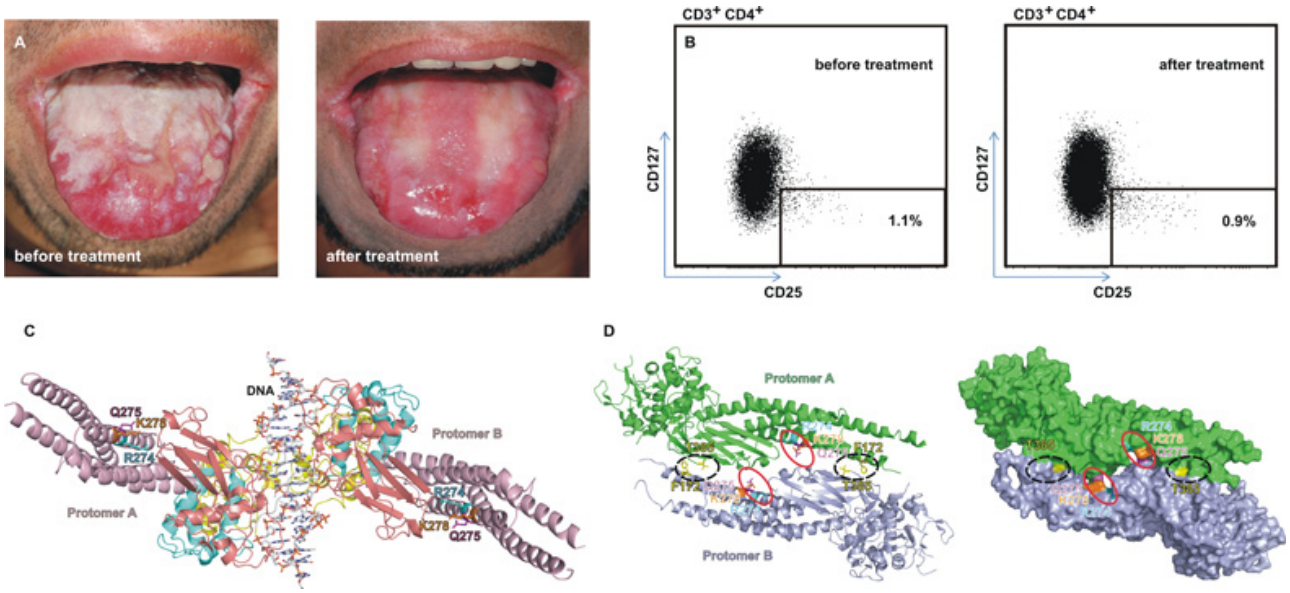

Fig. 1. Clinical efficacy of long-term administration of ruxolitinib in a CMC patient with a heterozygous STAT1 GOF mutation (R274Q) and localization of this and other important residues in the intradimeric interface connecting the two protomers in a parallel and antiparallel orientation. (A) Clinical images of the adult CMC patient carrying a pathogenic GOF missense mutation at position 274 before and 38 months after the start of the therapy with the JAK inhibitor ruxolitinib. (B) FACS analysis shows similar numbers of $CD3^+CD4^+CD25^{high}CD127^{low}$ T regulatory cells before (1.1%) and after (0.9%) ruxolitinib treatment. (C) Crystal structure of a truncated tyrosine-phosphorylated STAT1 dimer in parallel conformation showing the position of the side chains of R274 (light blue), Q275 (magenta), and K278 (orange) located in the coiled-coil domain. Structural data were obtained from the Protein Data Bank (pdb) file 1BF5 (Chen et al., 1998) using the program PyMOL (DeLano Scientific). (D) Ribbon diagram (left) and surface model (right) of the crystal structure of a truncated STAT1 dimer in antiparallel orientation showing two distinct binding areas in the dimer interface marked with dashed black ovals and red ovals, respectively. The known CMC-associated F172 and T385 residues are given in yellow. The PyMOL images were prepared using the pdb file 1 YV l (Mao et al., 2005). (For interpretation of the references to colour in this figure legend, the reader is referred to the web version of this article).

obstructive structures of the oesophagus (Mössner et al., 2016). Ruxolitinib therapy over 6 months resulted in an improved general health condition and increased numbers of total $CD4^+$ and $CD8^+$ T lymphocytes as well as B cells in the circulation. Here, we report that the continuous administration of the JAK inhibitor for additional 38 months further reduced oral thrush but did not lead to the complete resolution of mucositis in our patient (Fig. 1A). Despite the clinical efficacy of the drug treatment, the numbers of T regulatory cells, identified by flow cytometry as $CD3^+$ $CD4^+$ $CD25^{high}CD127^{low}$ peripheral cells, did not change during treatment (Fig. 1B). In the crystal structure of the DNA-bound STAT1 transcription factor (Mao et al., 2005), we noticed that the side chain of R274 in the coiled-coil domain points towards the interior of the STAT1 dimer, as do the neighbouring Q275 and the adjacent K278 (Fig. 1C). This sequence motif within the α-helix is highly conserved among the seven human STAT proteins and contains the pentapeptide structure R/Q-Q/R-Q/L/E-Ψ-K/E/R/G, where Ψ is a hydrophobic residue. In all human STAT family members with the exception of STAT6 (Q239), the first position in this surface-exposed sequence harbours an arginine, whereas in the second position there is always a glutamine residue (Q) except in STAT4 (R275), and in the fourth position there is a hydrophobic residue (leucine, isoleucine or valine). In the non-DNA-bound, antiparallel dimer, the residues R274, K278, and Q275 constitute two reciprocal finger-like bridge structures, which connect the two partner protomers at each side (Fig. 1D). This region localizes to the interior of the dimer interface and differs structurally from the well-stablished F172/T385 interaction known to also cause CMC when disrupted (Fig. 1D). Given the homology and clinical relevance of this sequence motif, we decided to introduce substitution mutations in the STAT1 four-helix bundle (R274W, Q275A, and K278A) and test the phenotype of the resulting three point mutants. Substitution of arginine 274 to tryptophan was chosen since this amino acid exchange has been linked to CMC (Soltész et al., 2013), and pathogenic GOF mutations at positions 275 and 278 have also been described (Yamazaki et al., 2014; Fujiki et al., 2017).

3.2. Elevated cytokine-induced tyrosine phosphorylation and DNA binding of the R274W and Q275A mutants

In order to compare the cellular effects of point mutations in the conserved α-helical coiled-coil domain, we reconstituted STAT1-negative U3A cells with mutant GFP fusion proteins of STAT1 and, 24 h post-transfection, stimulated the cells with 50 ng/ml of recombinant IFNγ for 45 min followed by exposure to the kinase inhibitor staurosporine (1 μM) for the indicated times. Western blotting demonstrated prolonged kinetics of tyrosine phosphorylation for the GFP-tagged STAT1-R274W mutant compared to the WT protein. Likewise, the Q275A mutant was partially resistant to the inhibitory effects of staurosporine on the kinetics of tyrosine phosphorylation, although this effect was less pronounced (Fig. 2A, B). In contrast, IFNγ-induced tyrosine phosphorylation of STAT1-K278A-GFP did not differ from STAT1-WT-GFP. Similar results were obtained in IFNγ-treated U3A cells expressing untagged variants, thus confirming previous observations of the hyperphosphorylated state of STAT1-R274W and extending these findings to the adjacent Q275A mutant (Fig. 2C, D). Again, the kinetics of STAT1-K278A was similar to the WT protein. Electrophoretic mobility shift assays (EMSA) using the same extracts as for Western blotting demonstrated the increased binding of the R274W and Q275A variants to a radioactively labelled probe with a consensus, single GAS sequence, whereas the lysine-to-alanine mutant was again undistinguishable from the WT protein (Fig. 2E, F). Time-course experiments using nuclear extracts from STAT1-expressing cells, treated for 45 min with IFNγ and subsequently for 20 and 60 min with staurosporine, confirmed the elevated GAS binding of both R274W and Q275A mutant proteins (Suppl. Fig. 1A).

3.3. Prolonged nuclear accumulation of the two point mutants in the four-helix bundle

Given the elevated tyrosine phosphorylation and increased binding

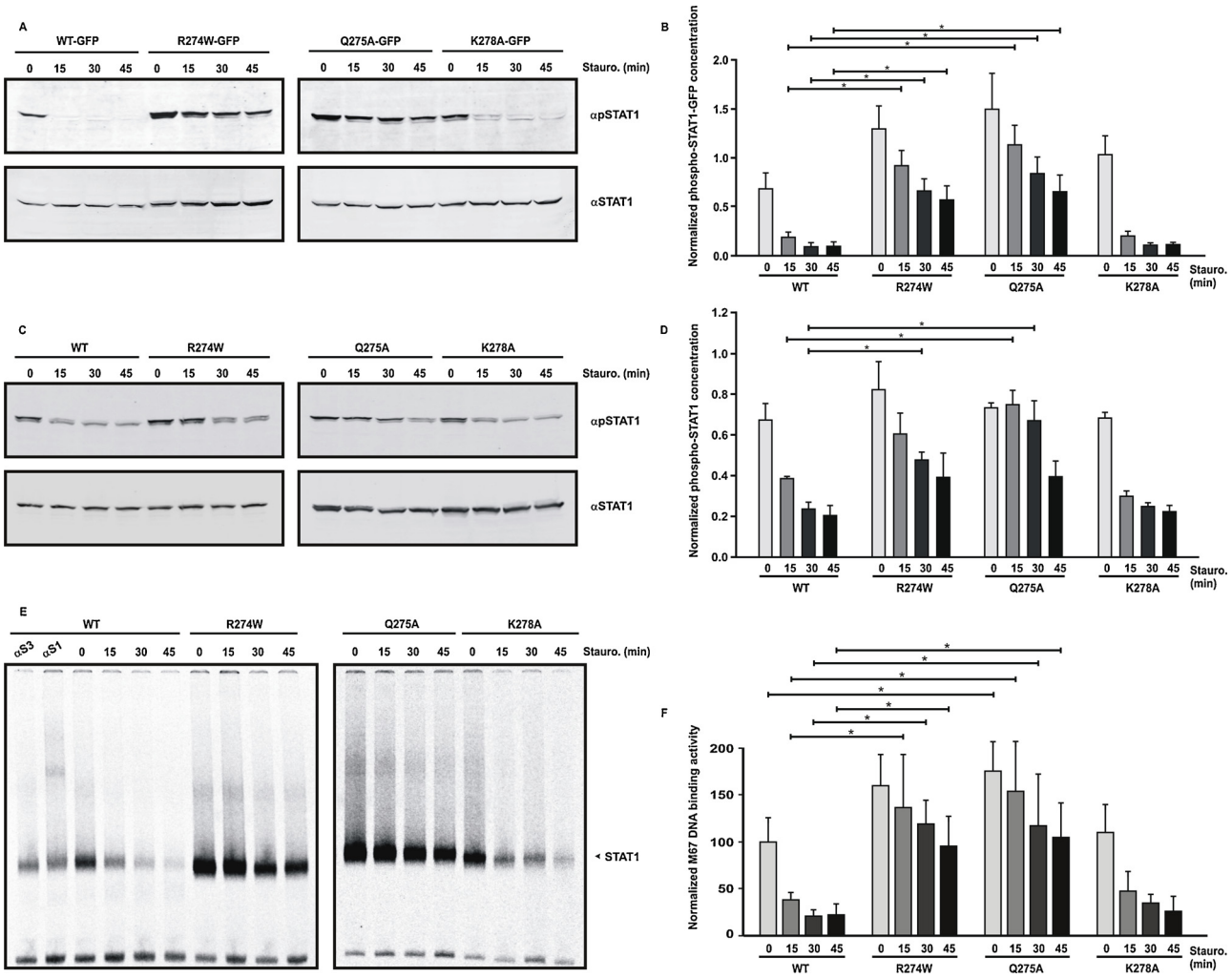

Fig. 2. Elevated tyrosine phosphorylation levels and DNA-binding activity of the R274W and Q275A mutants upon stimulation of cells with IFNγ. (A, B) Transfected STAT1-negative U3A cells expressing GFP-fusion proteins of wild-type (WT) or mutant STAT1 were treated for 45 min with 50 ng/ml of recombinant IFNγ followed by incubation with the kinase inhibitor staurosporine (1 μM) for the indicated times. (A) Representative Western blot results from whole cell extracts probed with a phosphotyrosine-specific STAT1 antibody (αpSTAT1) and, after re-exposure of the same membranes, to a pan-STAT1 antibody (αSTAT1). (B) Quantification of the Western-Blot results from three independent transfection experiments, as shown in (A). Asterisks indicate significant differences between the WT protein and the respective mutants. (C, D) Immunoblotting results from reconstituted U3A cells expressing untagged STAT1 proteins confirmed the hyper-phosphorylation of R274W and Q275A (n = 3). (E, F) Electrophoretic mobility shift assay demonstrated increased binding of the R274W and Q275A variants from whole cell extracts to a [^{33}P]-radioactively labelled M67 probe containing a consensus, single GAS sequence, whereas the K278A mutant showed no altered DNA-binding kinetics as compared to the WT molecule. Autoradiograms show a representative EMSA result (E) and the quantification thereof from three independent transfection experiments (F).

to a single GAS site of the R274W and Q275A mutants, we next examined the kinetics of their nuclear accumulation in IFNγ-stimulated cells by means of epifluorescence microscopy. All four GFP-tagged STAT1 variants under investigation displayed a similar cellular distribution with a predominantly cytoplasmic localization in resting cells, and treatment with IFNγ for 45 min resulted in their nuclear accumulation (Fig. 3A). While a 30-minute exposure to staurosporine restored the resting distribution of STAT1-WT-GFP and STAT1-K278A-GFP in IFNγ-pretreated cells, the R274W and Q275A mutants were insensitive to the inhibitory effect of staurosporine for at least 1 h after their cytokine-induced nuclear accumulation (Fig. 3A, B). The staurosporine insensitivity of R274W and Q275A was observed not only for fusions with GFP in HeLa cells (Fig. 3A, B), but also for recombinant untagged STAT1 proteins expressed in reconstituted STAT1-negative U3A cells (Fig. 3C, D). In addition to the prolonged nuclear accumulation of the two R274W and Q275A mutants in IFNγ-treated cells, we observed that their nuclear accumulation occurred in a short time period after adding of the cytokine to the cells (Fig. 3E, F, Suppl. Fig. 1B). While it took only 10 min of IFNγ stimulation to induce complete nuclear accumulation for R274W and Q275A, additional 10 min were required for the WT molecule and the K278A mutant. In summary, the R274W and Q275A variants showed a faster nuclear retention and prolonged nuclear accumulation phase upon treatment of cells with IFNγ.

3.4. Increased gene activation of point mutants in the STAT1 coiled-coil domain

In the next set of experiments, we assessed the impact of the coiled-coil domain mutations on gene expression using reporter and real-time RT-PCR assays in reconstituted U3A cells stimulated with IFNγ. These experiments confirmed that substitution of the arginine residue normally present at position 274 results in a GOF phenotype, and, in addition, showed that this is also the case for the Q275A mutation (Fig. 4). Unexpectedly, we found that the K278A mutant, which did not differ from the WT molecule with respect to tyrosine phosphorylation (Fig. 2A-D), GAS binding (Fig. 2E, F), and the kinetics of nuclear accumulation (Fig. 3), was a better transcriptional activator at three of the four tested endogenous STAT1 target genes, namely *MIG1*, *IRF1*, and

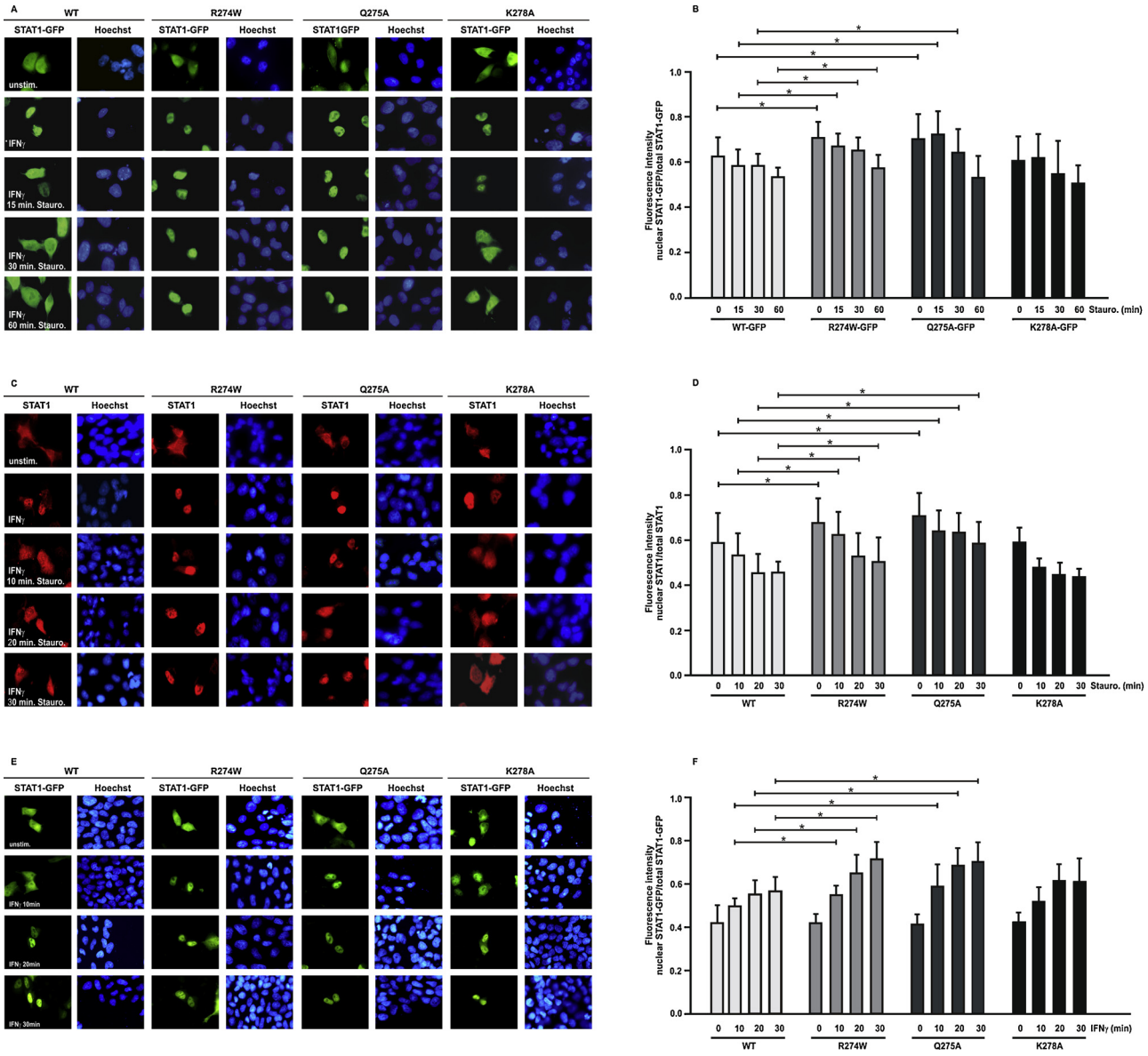

Fig. 3. Premature and prolonged accumulation of STAT1-R274W and -Q275A in the nuclei of IFNγ-treated cells. (A, B) HeLa cells expressing the indicated STAT1-GFP fusion proteins were either left unstimulated or stimulated for 45 min with human IFNγ (50 ng/ml) followed by exposure to staurosporine (1 μM) for 0 min, 15 min, 30 min and 60 min, respectively. (A) The fluorescence micrographs show the intracellular distribution of GFP-tagged STAT1 for the indicated variants as well as the localization of the corresponding Hoechst-stained nuclei (n = 3 independent transfections). (B) Histograms demonstrate the nucleocytoplasmic STAT1-GFP distribution in untreated cells and IFNγ-pretreated cells exposed to staurosporine for the increasing times, as determined by the ratio of nuclear-to-total fluorescence intensity. (C, D) Indirect fluorescence microscopy confirmed the prolonged nuclear accumulation phase of untagged R274W and Q275A. STAT1-negative U3A cells were transfected with plasmids coding for WT or mutant STAT1 and, on the next day, treated as described above, except that the exposure times to staurosporine were shortened (0 min, 10 min, 20 min, and 30 min). (C) The intracellular distribution of recombinant STAT1 was monitored immunocytochemically in the methanol-fixed, Hoechst-stained cells using anti-STAT1 (E-23) primary and Cy3-labelled secondary antibodies (n = 3). (D) Nucleocytoplasmic distribution of the STAT1 mutants, as quantified from Fig. 3C, with bars and asterisks indicating significant differences between WT and mutant STAT1. (E, F) Premature nuclear accumulation of R274W-GFP and Q275A-GFP in HeLa cells occurs already 10 min after IFNγ treatment, whereas it took 10 min longer for the WT and the K278A protein to achieve a complete accumulation state (n = 3).

CCL2, but not *CXCL10* (Fig. 4C-F). Control experiments demonstrated that the altered gene activation profile of the K278A mutant was not due to an elevated expression of the mutant, since the *STAT1* mRNA levels were similar between cells expressing the recombinant WT and mutant STAT1 (Fig. 4G). Although GAS binding was increased in reconstituted U3A cells exposed for 20 min to IFNα (Supplemental Fig. 2A, B) and, moreover, IFNα stimulation significantly up-regulated the expression of IFN type-I-driven genes (Supplemental Fig. 2C), we observed no significant differences among the STAT1 variants with respect to activation of the three IFNα-driven genes *RIG-G*, *IFI-56 K* and *MX1* (Supplemental Fig. 2C).

3.5. Normal DNA-binding affinity of the coiled-coil domain mutants

Given the altered expression profile of the three mutants R274W, Q275A, and K278A on endogenous IFNγ-driven target genes, we next evaluated their sequence-specific binding kinetics to DNA. In a first competition experiment, the dissociation rate from a high-affinity, single GAS site, termed M67, was tested for the WT and mutant STAT1 proteins. To this end, whole cell extracts from STAT1-expressing U3A cells were incubated for 15 min with [^{33}P]-labelled M67 DNA, before the reactions were either unchallenged (0 min) or challenged with a 750-fold molar excess of unlabelled M67 for additional 5 or 10 min on

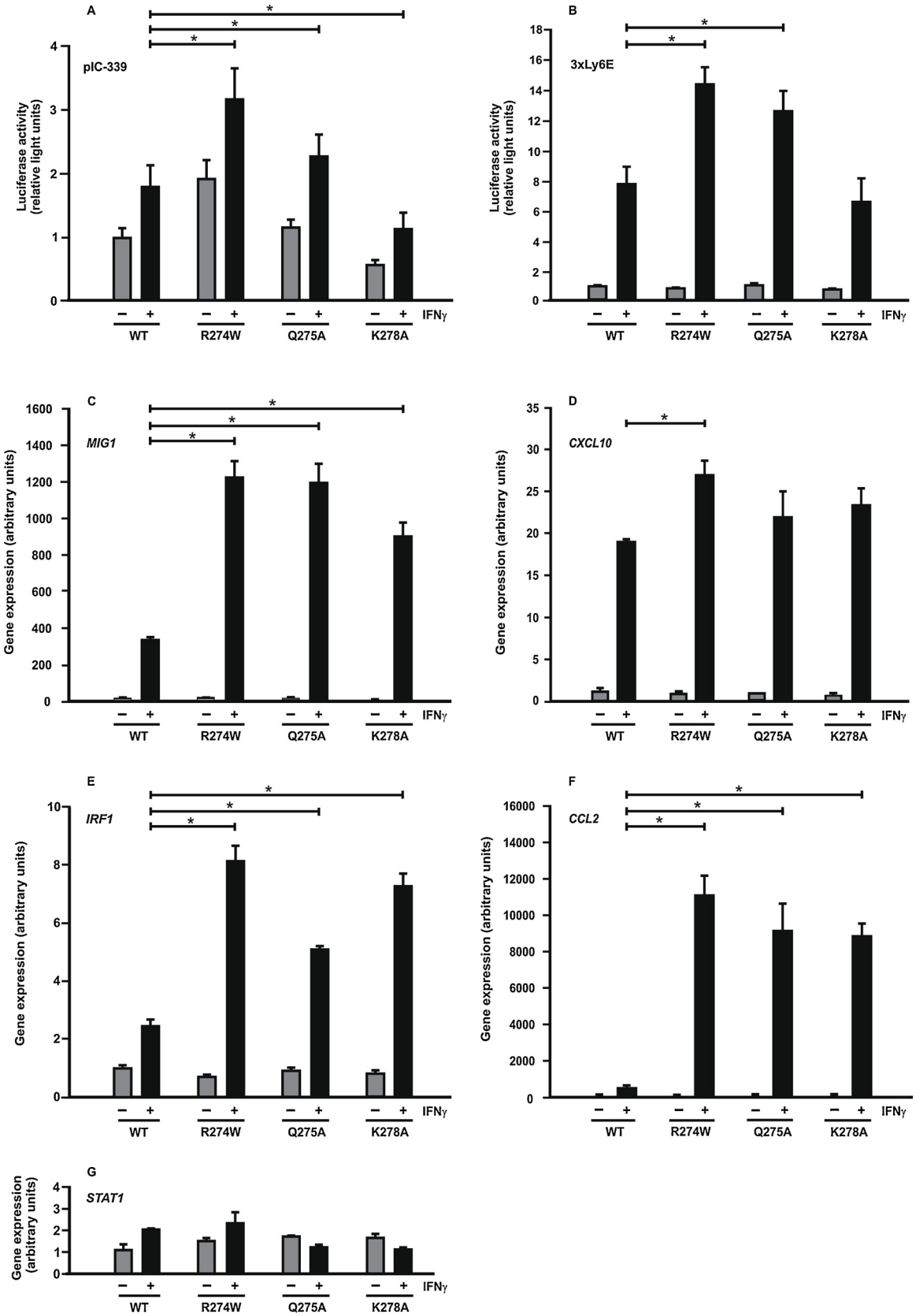

(caption on next page)

Fig. 4. Gene-specific expression patterns demonstrate that R274W and Q275A are hyper-active inducers of transcriptional responses, while K278A functions as a moderate GOF mutant for endogenous target genes. (A, B) Luciferase reporter gene assays in reconstituted U3A cells expressing the indicated STAT1 variants normalized to the expression level of constitutively co-expressed β-galactosidase. The reporter constructs used in these experiments contained inserts from either (A) a 339 base pair fragment from the native *ICAM-1* promoter (pIC-339) or (B) a triple GAS site from the *Ly6E* promoter (3xLy6E). Cells were left untreated (grey columns) or stimulated for 6 h (black) with 50 ng/ml of IFNγ before, in whole cell extracts, luciferase luminescence and the enzymatic activity of the co-expressed β-galactosidase were measured. The experiment was repeated in six independent transfections at least three times. (C–G) Endogenous gene expression by the indicated STAT1 mutants was determined by real-time RT-PCR assays. Histograms depict expression levels of the *MIG1* (C), *CXCL10* (D), *IRF1* (E), *CCL2* (F), and *STAT1* (G) gene before (grey columns) and after 6 h stimulation with IFNγ (black columns). Gene induction was normalized to the expression of the house-keeping gene *GAPDH*. Histograms show means and standard deviations. Significant differences for IFNγ-stimulated samples expressing the indicated STAT1 mutants in comparison to the WT protein are marked by bars and asterisks. The experiment was repeated three times.

ice, before being loaded on a non-denaturing gel. EMSA revealed that the three mutants displayed similar dissociation kinetics from a high-affinity GAS site as the WT protein (Fig. 5A, B). Furthermore, all four STAT1 variants showed cooperative DNA binding, as tetrameric but not dimeric STAT1 complexes resisted binding to a radioactively labelled DNA probe containing two consensus GAS sites in tandem orientation, when challenged for 30 min with a 750-fold molar excess of unlabelled GAS (Fig. 5C, D). Likewise, the STAT1 mutants did not differ from the WT protein with respect to binding to tandem GAS sites of different sequence-specificity (Fig. 5E, F). Thus, the elevated gene activation of the three coiled-coil domain mutants cannot be explained by altered DNA binding.

3.6. R274W and Q275A display unaltered kinetics of tyrosine phosphorylation and dephosphorylation

The preceding experiments had indicated that the two hyper-phosphorylated STAT1 GOF mutants R274W and Q275A had a more pronounced cytokine-inducible nuclear accumulation (Fig. 3), but displayed normal kinetics of GAS binding (Fig. 5). Finally, we questioned whether the hyper-phosphorylated status of these mutants in IFNγ-stimulated cells results from either elevated tyrosine phosphorylation by JAKs and/or impaired dephosphorylation by the STAT1-inactivating Tc45 phosphatase. To test this hypothesis, we prepared cellular extracts from untreated U3A cells expressing either WT or mutant STAT1 and incubated the samples *in vitro* with the recombinant JAK2 kinase for 0, 30, and 60 min. As shown in Fig. 6A and B, all coiled-coil domain mutants were normally phosphorylated by JAK2. Likewise, when extracts from IFNγ-pretreated U3A cells expressing the respective phosphorylated STAT1 mutants were incubated with recombinant Tc45 phosphatase, their dephosphorylation rates were similar to WT protein (Fig. 6C, D). These observations demonstrated that the elevated tyrosine phosphorylation levels of R274W and Q275A resulted neither from an improved interaction with JAK2 nor from an impaired reaction with Tc45. Since it is well established that DNA binding protects STAT1 from being dephosphorylated by the inactivating phosphatase (Meyer et al., 2003), we finally tested the mutants in an *in vitro* dephosphorylation assay using purified Tc45 in the absence or presence of GAS-containing, double-stranded DNA. As shown in Fig. 6E and F, the presence of a high-affinity GAS-nonGAS element in the reactions protected all four STAT1 variants from being dephosphorylated, whereas the same molar concentration of unspecific 2xnonGAS did not prevent phospho-STAT1 from being inactivated by the catalytic action of the phosphatase. Again, the dephosphorylation patterns of the mutants did not differ from the WT protein.

4. Discussion

In the present study, we extend our knowledge about the molecular mechanisms of the CMC pathogenic R274 substitution by showing that this mutation, similar to the adjacent missense mutation Q275A, leads to an early and prolonged nuclear accumulation upon stimulation of cells with the cytokine IFNγ. Both point mutants were hyper-phosphorylated and insensitive towards the inhibitory effects of staurosporine, resulting in a higher occupancy rate on GAS elements. A detailed molecular characterization of the two mutants revealed that neither the rate of JAK2-induced tyrosine phosphorylation, nor the kinetics of DNA-binding was per se affected by the missense mutations. Furthermore, the dissociation rate from a classical GAS element, tetramer formation, and sequence-specificity did not differ between WT and mutant proteins. These kinetic observations are in line with the findings from genome-wide RNA-sequencing libraries by Fujiki and colleagues demonstrating that the aberrant increase in STAT1 activity was not associated with a significant change in the repertoire of STAT1 target genes (Fujiki et al., 2017). The development of CMC was attributed to an impaired Th17 immunity, although the precise molecular mechanisms have not been elucidated. Yamazaki et al. (2014) demonstrated that the production of the Th17-associated cytokines IL-17A and IL-22 from peripheral blood mononuclear cells (PBMCs) and $CD4^+$ T cells was significantly reduced in patients with STAT1 GOF mutations. The decreased synthesis of IL-17A and IL-22 indicates an impaired differentiation of Th17 cells and suggests non-redundant roles of Th17 cells and Th17-associated cytokines in the host defence against mucocutaneous Candida infections.

The main observation of this study is that the two hyper-phosphorylated R274W and Q275A mutations, both located at the interface of the antiparallel dimer, exhibited unaltered phosphorylation and dephosphorylation reactions, when the mutants were incubated with the activating JAK2 kinase and the inactivating Tc45 phosphatase, respectively. This behaviour clearly distinguishes the two R274W and Q275A mutants from F172W, F364A, and T385A, which are also hyper-phosphorylated, but have been shown by our group to be resistant against the dephosphorylation effects of the Tc45 phosphatase, when tested under the same experimental conditions (Staab et al., 2013a,b). These latter residues are required for the formation of the antiparallel dimer conformation, which cannot be stabilized when they are mutated (Zhong et al., 2005; Mertens et al., 2006; Staab et al., 2013a,b). The functional consequences of the K278A substitution with regard to hyper-phosphorylation seem to be less pronounced than the other two GOF mutants. However, this STAT1 variant should also be classified as a GOF mutant, given its elevated gene activation profile on a variety of IFNγ-driven target genes.

Our work has identified two different categories of hyper-active GOF mutations, which differ with regard to their Tc45-induced dephosphorylation properties as well as their location in distinct areas of the interface constituting the antiparallel STAT1 dimer conformer. The amino acid residues constituting the phosphatase-insensitive mutants F172W, F364A, and T385A are located at the periphery of the interface, whereas the newly identified phosphatase-sensitive mutant Q275A and its neighbour R274W are both located in the centre of the antiparallel dimer (Fig. 1D). Thus, the two functionally distinguishable groups of GOF mutations can be clearly assigned to different areas of the antiparallel dimer conformation, as the phosphatase-sensitive mutations characterized in this paper are disrupting the formation of an isolated, finger-like structure naturally occurring at the dimer interface. X-ray crystallographic studies of the antiparallel STAT1 conformation (Mao et al., 2005) reveal that the side chain of glutamine 275 is only 3.2 Å apart from the aromatic ring system of the tyrosine residue Y356 on the partner protomer, which most likely contributes to the formation of a nonphosphorylated STAT1 dimer. Furthermore, our results suggest that

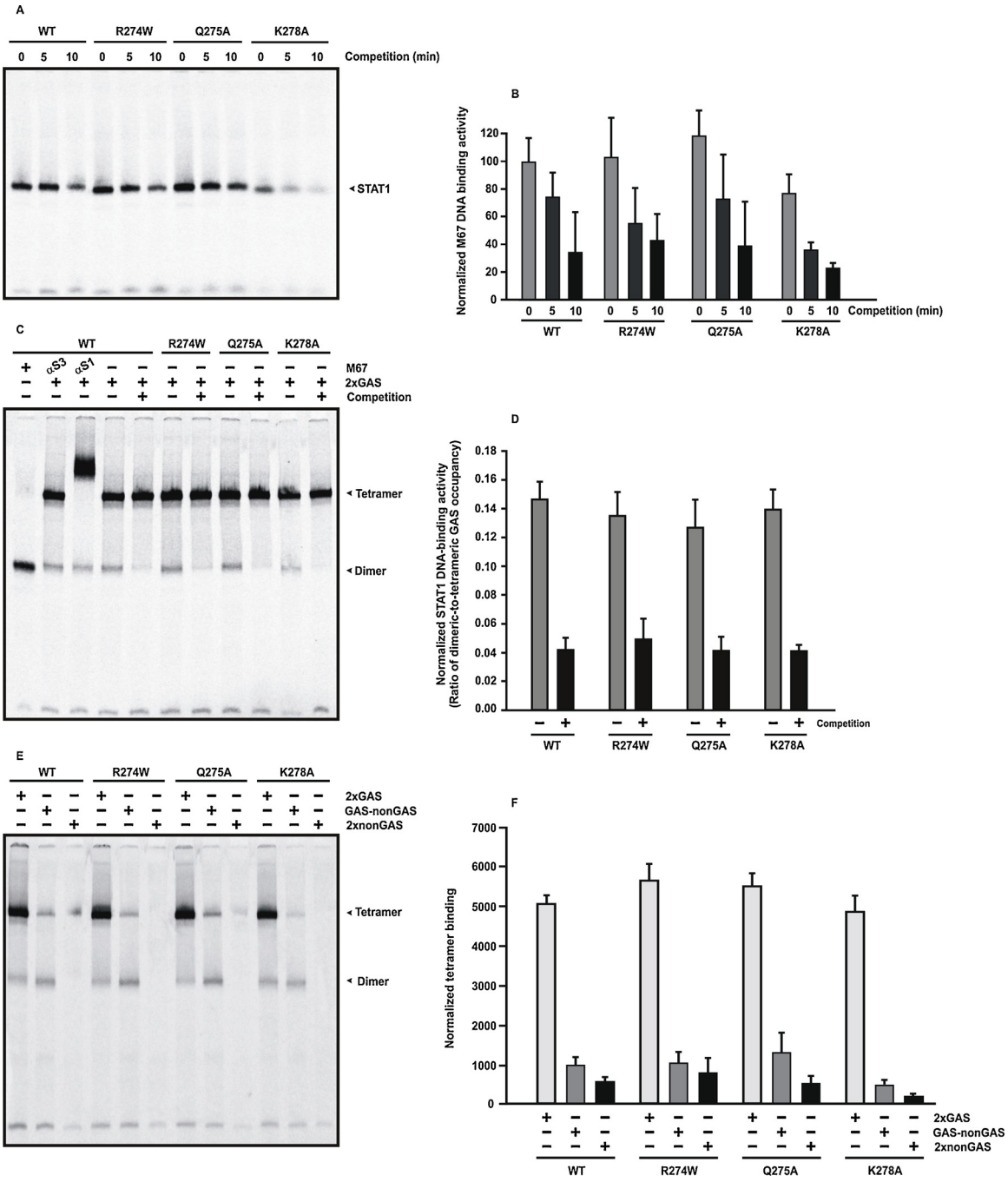

Fig. 5. Normal sequence-specific binding of the GOF mutants to DNA. (A, B) Unaltered dissociation kinetics from GAS sites for the tested GOF mutants, as demonstrated by means of a competition gel-shift assay. Lysates from cells expressing the indicated tyrosine-phosphorylated STAT1 variants were equilibrated for 15 min with a radioactively labelled high-affinity STAT-binding probe termed M67, before a 750-fold molar excess of unlabelled M67 was added on ice for 5 min and 10 min, respectively, and the reactions loaded on a non-denaturing gel. A representative autoradiogram of the competition gel-shift is shown in (A), including the quantification from three independent experiments thereof (B). (C, D) Cooperative DNA binding resulting from tetramer stability is unaltered in the GOF mutants. (C) The image shows a representative EMSA result using whole cell extracts from reconstituted U3A cells incubated with a [^{33}P]-labelled double-stranded oligonucleotide containing two GAS elements in tandem orientation (2xGAS) with the positions of tetrameric and dimeric STAT1 indicated at the right-hand margin of the gel. Reactions were either unchallenged (-) or challenged with a 750-fold molar excess of unlabelled GAS (+ competition). Where indicated, an anti-STAT3 (αS3) or anti-STAT1 antibody (αS1) was included in the reaction. To identify the position of dimeric STAT1, a [^{33}P]-labelled single GAS site (M67) was included in the first lane. (D) The percentage of dimeric-to-tetrameric STAT1 complexed to 2xGAS did not differ among the four STAT1 variants tested (n = 3). (E, F) GOF mutants have a similar sequence-specific DNA-binding affinity as the WT protein. Extracts from U3A cells expressing the indicated STAT1 variants were incubated with [^{33}P]-labelled double-stranded DNA containing two (2xGAS), one (GAS-nonGAS) or none (2xnonGAS) GAS sites and proceeded for EMSA. (E) Representative gel-shift and (F) data from densitometric analysis from three independent experiments.

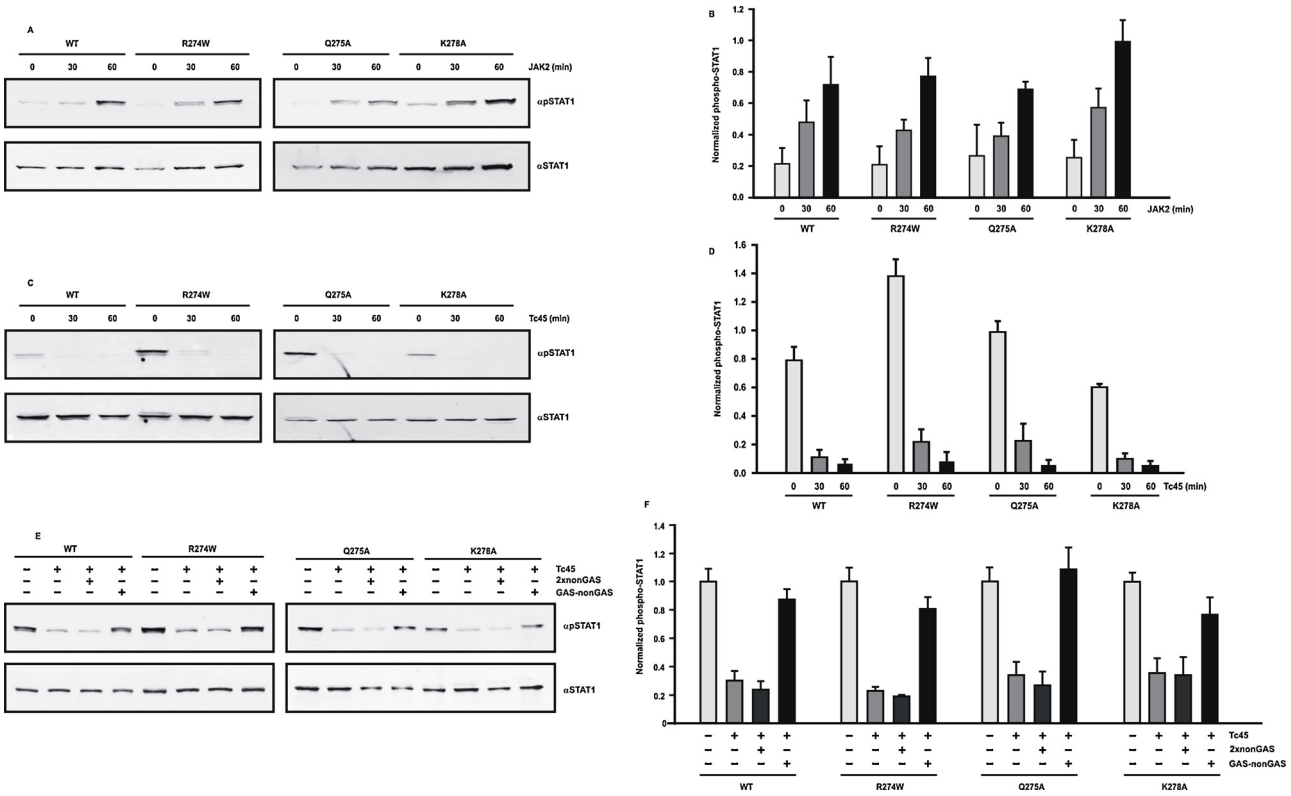

Fig. 6. The substitution mutants R274W, Q275A and K278A in the coiled-coil domain display unaltered *in vitro* phosphorylation and dephosphorylation kinetics. (A) *In vitro* phosphorylation assay demonstrated no different tyrosine phosphorylation rates of the STAT1 variants by JAK2. Whole cell extracts from reconstituted U3A cells expressing STAT1 (10 µl in each reaction) were incubated with 4 µg/ml of recombinant JAK2 kinase and incorporation of phosphate in STAT1 was monitored over time by means of Western blotting (n = 3). (B) Statistical analysis revealed no significant difference in the phosphorylation kinetics between WT and mutant STAT1. (C) The GOF mutants are normally dephosphorylated by Tc45 phosphatase. Results from an *in vitro* dephosphorylation assay using extracts from IFNγ – prestimulated U3A cells (10 µl each) incubated for 0, 30 and 60 min with 2 U of the STAT1-specific Tc45 phosphatase (n = 3). Tyrosine dephosphorylation was followed by immunoblotting (C) including a quantitative analysis of the phosphotyrosine signals divided by the total STAT1 signal (D). (E, F) The GOF mutants are normally protected against the inactivating effect of Tc45 phosphatase when bound to high-affinity GAS elements. Results from an *in vitro* dephosphorylation assay in the presence of GAS-nonGAS and 2xnonGAS double-stranded oligonucleotides (n = 3).

there is more than one distinct mechanism responsible for the hyperactive properties of GOF mutants.

The identification of functionally different GOF mutants may help in future experiments to better understand the molecular basis of the important activating/inactivation cycle required for STAT1 to function as a cytokine-inducible transcription factor. One possible hypothesis from our observations is that the reciprocal F172/T385 interaction located at the lateral ends of the antiparallel dimer interface is required for the formation of isolated dimers (or multimers) of antiparallel STAT1, which then recruit the Tc45 phosphatase as a prerequisite for its enzymatic action on STAT1. In contrast, the second binding site of the antiparallel dimer with the R274/Q275 bridge structure may be involved in the binding of a single STAT1 monomer (or a parallel phospho-dimer) to a tyrosine-phosphorylated dimer in an antiparallel conformation. This hypothetical trimeric complex may exclude the binding of importin-α to the dimer-specific nuclear localisation signal (NLS) located at the DNA-binding domain (Meyer et al., 2002), which is masked by the coiled-coil domain of the interfering third protomer.

According to this theory, importin-α5 and STAT1 compete for binding to a phosphorylated homodimer. The model implies that the nuclear import of tyrosine-phosphorylated STAT1 dimers is hindered by monomeric STAT1 irrespective of its phosphorylation state. According to this assumption, the second interface with the R274/Q275 residues is engaged in the formation of a trimeric complex by binding a STAT1 monomer (or dimer) in an antiparallel conformation to one of the two STAT1 protomers which constitute a parallel dimer *via* reciprocal phospho-tyrosine-SH2 domain interactions. The physiological consequence of such a hypothetical mechanism would be that monomeric STAT1 functions as an inhibitor for the import of dimeric phospho-STAT1 by setting a high threshold for the intracellular concentration of phosphorylated STAT1 to enter the nucleus and execute transcriptional responses. The inhibitory function of monomeric STAT1 would assure that STAT1 nuclear accumulation is promoted in cells exposed to high concentrations of extracellular cytokines. It remains speculative whether a high rate of receptor occupancy is required in order to overcome the putative antagonistic effects of the trimeric STAT1 complex.

Our epifluorescence microscopic observation that the R274W and Q275A mutants are rapidly imported into the nucleus after stimulation of the cells with cytokines supports this assumption. However, further experiments are required to decipher the molecular basis of these interesting and clinically relevant GOF mutations. In addition, the speculative model has to be tested that indeed monomeric, unphosphorylated STAT1 prevents the nuclear import of phosphorylated STAT1 simply by hindering the access of importin molecules to STAT1 dimers as a prerequisite for nuclear import and full-fledged transcriptional responses.

Declaration of Competing Interest

None.

Acknowledgement and funding

The authors gratefully acknowledge the excellent technical assistance of Anke Gregus and Heike Hühn. We kindly thank Professor Uwe Vinkemeier, University of Nottingham, for valuable reagents and discussions. The research on this subject was funded by grants from the Deutsche Forschungsgemeinschaft to the International Research Training Group (IRTG) 1618 “Phosphorylation- and redox-mediated signalling mechanisms in the failing heart”, which is a cooperation between the Medical Faculty of the University of Göttingen and the BHF Centre of Research Excellence at King´s College London (RE/13/2/30182). The project was also funded by a grant from the Nachlass der Frau Lore Grun.

Appendix A. Supplementary data

Supplementary material related to this article can be found, in the online version, at doi:https://doi.org/10.1016/j.molimm.2019.07.008.

References

Begitt, A., Meyer, T., van Rossum, M., Vinkemeier, U., 2000. Nucleocytoplasmic translocation of Stat1 is regulated by a leucine-rich export signal in the coiled-coil domain. Proc. Natl. Acad. Sci. U.S.A. 97, 10418–10423.

Chen, X., Vinkemeier, U., Zhao, Y., Jeruzalmi, D., Darnell Jr., J.E., Kuriyan, J., 1998. Crystal structure of a tyrosine phosphorylated STAT-1 dimer bound to DNA. Cell 93, 827–839.

Decker, T., Kovarik, P., Meinke, A., 1997. GAS elements: a few nucleotides with a major impact on cytokine-induced gene expression. J. Interferon Cytokine Res. 17, 121–134.

Depner, M., Fuchs, S., Raabe, J., Frede, N., Glocker, C., Doffinger, R., Gkrania-Klotsas, E., Kumararatne, D., Atkinson, T.P., Schroeder, H.W., Niehues, T., Dückers, G., Stray-Pedersen, A., Baumann, U., Schmidt, R., Franco, J.L., Orrego, J., Ben-Shoshan, M., McCusker, C., Jacob, C.M., Carneiro-Sampaio, M., Devlin, L.A., Edgar, J.D., Henderson, P., Russell, R.K., Skytte, A.B., Seneviratne, S.L., Wanders, J., Stauss, H., Meyts, I., Moens, L., Jesenak, M., Kobbe, R., Borte, S., Borte, M., Wright, D.A., Hagin, D., Torgerson, T.R., Grimbacher, B., 2016. The extended clinical phenotype of 26 patients with chronic mucocutaneous candidiasis due to gain-of-function mutations in STAT1. J. Clin. Immunol. 36, 73–84.

Dupuis, S., Dargemont, C., Fieschi, C., Thomassin, N., Rosenzweig, S., Harris, J., Holland, S.M., Schreiber, R.D., Casanova, J.L., 2001. Impairment of mycobacterial but not viral immunity by a germline human STAT1 mutation. Science 293, 300–303.

Dupuis, S., Jouanguy, E., Al-Hajjar, S., Fieschi, C., Al-Mohsen, I.Z., Al-Jumaah, S., Yang, K., Chapgier, A., Eidenschenk, C., Eid, P., Al Ghonaium, A., Tufenkeji, H., Frayha, H., Al-Gazlan, S., Al-Rayes, H., Schreiber, R.D., Gresser, I., Casanova, J.L., 2003. Impaired response to interferon-α/β and lethal viral disease in human *STAT1* deficiency. Nat. Genet. 33, 388–391.

Fujiki, R., Hijikata, A., Shirai, T., Okada, S., Kobayashi, M., Ohara, O., 2017. Molecular mechanism and structural basis of gain-of-function of STAT1 caused by pathogenic R274Q mutation. J. Biol. Chem. 292, 6240–6254.

Haspel, R.L., Darnell, J.E., 1999. A nuclear protein tyrosine phosphatase is required for the inactivation of Stat1. Proc. Natl. Acad. Sci. U.S.A. 96, 10188–10193.

Levy, D.E., Darnell, J.E., 2002. Stats: transcriptional control and biological impact. Nat. Rev. Mol. Cell Biol. 3, 651–662.

Liu, L., Okada, S., Kong, X.F., Kreins, A.Y., Cypowyj, S., Abhyankar, A., Toubiana, J., Itan, Y., Audry, M., Nitschke, P., Masson, C., Toth, B., Flatot, J., Migaud, M., Chrabieh, M., Kochetkov, T., Bolze, A., Borghesi, A., Toulon, A., Hiller, J., Eyerich, S., Eyerich, K., Gulácsy, V., Chernyshova, L., Chernyshov, V., Bondarenko, A., Grimaldo, R.M., Blancas-Galicia, L., Beas, I.M., Roesler, J., Magdorf, K., Engelhard, D., Thumerelle, C., Burgel, P.R., Hoernes, M., Drexel, B., Seger, R., Kusuma, T., Jansson, A.F., Sawalle-Belohradsky, J., Belohradsky, B., Jouanguy, E., Bustamante, J., Bué, M., Karin, N., Wildbaum, G., Bodemer, C., Lortholary, O., Fischer, A., Blanche, S., Al-Muhsen, S., Reichenbach, J., Kobayashi, M., Rosales, F.E., Lozano, C.T., Kilic, S.S., Oleastro, M., Etzioni, A., Traidl-Hoffmann, C., Renner, E.D., Abel, L., Picard, C., Maródi, L., Boisson-Dupuis, S., Puel, A., Casanova, J.L., 2011. Gain-of-function human *STAT1* mutations impair IL-17 immunity and underlie chronic mucocutaneous candidiasis. J. Exp. Med. 208, 1635–1648.

Mao, X., Ren, Z., Parker, G.N., Sondermann, H., Pastorello, M.A., Wang, W., McMurray, J.S., Demeler, B., Darnell Jr, J.E., Chen, X., 2005. Structural bases of unphosphorylated STAT1 association and receptor binding. Mol. Cell 17, 761–771.

Mertens, C., Zhong, M., Krishnaraj, R., Zou, W., Chen, X., Darnell, J.E., 2006. Dephosphorylation of phosphotyrosine on STAT1 dimers requires extensive spatial reorientation of the monomers facilitated by the N-terminal domain. Genes Dev. 20, 3372–3381.

Meyer, T., Begitt, A., Lödige, I., van Rossum, M., Vinkemeier, U., 2002. Constitutive and IFNγ-induced nuclear import of STAT1 proceed through independent pathways. EMBO J. 21, 344–354.

Meyer, T., Marg, A., Lemke, P., Wiesner, B., Vinkemeier, U., 2003. DNA binding controls inactivation and nuclear accumulation of the transcription factor Stat1. Genes Dev. 17, 1992–2005.

Mössner, R., Diering, N., Bader, O., Forkel, S., Overbeck, T., Gross, U., Grimbacher, B., Schön, M.P., Buhl, T., 2016. Ruxolitinib induces interleukin 17 and ameliorates chronic mucocutaneous candidiasis caused by STAT1 gain-of-function mutation. Clin. Infect. Dis. 62, 951–953.

Müller, M., Laxton, C., Briscoe, J., Schindler, C., Improta, T., Darnell, J.E., Stark, G.R., Kerr, I.M., 1993. Complementation of a mutant cell line: central role of the 91 kDa polypeptide of ISGF3 in the interferon-α and -ɣ signal transduction pathways. EMBO J. 12, 4221–4228.

Seddiki, N., Santner-Nanan, B., Martinson, J., Zaunders, J., Sasson, S., Landay, A., Solomon, M., Selby, W., Alexander, S.I., Nanan, R., Kelleher, A., Fazekas de St Groth, B., 2006. Expression of interleukin (IL)-2 and IL-7 receptors discriminates between human regulatory and activated T cells. J. Exp. Med. 203, 1693–1700.

Shuai, K., Schindler, C., Prezioso, V.R., Darnell, J.E., 1992. Activation of transcription by IFN-gamma: tyrosine phosphorylation of a 91-kD DNA binding protein. Science 258, 1808–1812.

Shuai, K., Horvath, C.M., Huang, L.H., Qureshi, S.A., Cowburn, D., Darnell, J.E., 1994. Interferon activation of the transcription factor Stat91 involves dimerization through SH2-phosphotyrosyl peptide interactions. Cell 76, 821–828.

Soltész, B., Tóth, B., Shabashova, N., Bondarenko, A., Okada, S., Cypowyj, S., Abhyankar, A., Csorba, G., Taskó, S., Sarkadi, A.K., Méhes, L., Rozsíval, P., Neumann, D., Chernyshova, L., Tulassay, Z., Puel, A., Casanova, J.L., Sediva, A., Litzman, J., Maródi, L., 2013. New and recurrent gain-of-function *STAT1* mutations in patients with chronic mucocutaneous candidiasis from Eastern and Central Europe. J. Med. Genet. 50, 567–578.

Staab, J., Herrmann-Lingen, C., Meyer, T., 2013a. A rapid conformational rearrangement of STAT1 dimers is required for termination rather than for amplification of interferon-γ signaling. JAKSTAT 2, e23576.

Staab, J., Herrmann-Lingen, C., Meyer, T., 2013b. Clinically relevant dimer interface mutants of STAT1 transcription factor exhibit differential gene expression. PLoS One 8, e69903.

ten Hoeve, J., de Jesus Ibarra-Sanchez, M., Fu, Y., Zhu, W., Tremblay, M., David, M., Shuai, K., 2002. Identification of a nuclear Stat1 protein tyrosine phosphatase. Mol. Cell. Biol. 22, 5662–5668.

Toubiana, J., Okada, S., Hiller, J., Oleastro, M., Lagos Gomez, M., Aldave Becerra, J.C., Ouachée-Chardin, M., Fouyssac, F., Girisha, K.M., Etzioni, A., van Montfrans, J., Camcioglu, Y., Kerns, L.A., Belohradsky, B., Blanche, S., Bousfiha, A., Rodriguez-Gallego, C., Meyts, I., Kisand, K., Reichenbach, J., Renner, E.D., Rosenzweig, S., Grimbacher, B., van de Veerdonk, F.L., Traidl-Hoffmann, C., Picard, C., Marodi, L., Morio, T., Kobayashi, M., Lilic, D., Milner, J.D., Holland, S., Casanova, J.L., Puel, A., International STAT1 Gain-of-Function Study Group, 2016. Heterozygous *STAT1* gain-of-function mutations underlie an unexpectedly broad clinical phenotype. Blood 127, 3154–3164.

van de Veerdonk, F.L., Plantinga, T.S., Hoischen, A., Smeekens, S.P., Joosten, L.A., Gilissen, C., Arts, P., Rosentul, D.C., Carmichael, A.J., Smits-van der Graaf, C.A., Kullberg, B.J., van der Meer, J.W., Lilic, D., Veltman, J.A., Netea, M.G., 2011. *STAT1* mutations in autosomal dominant chronic mucocutaneous candidiasis. N. Engl. J. Med. 365, 54–61.

Yamazaki, Y., Yamada, M., Kawai, T., Morio, T., Onodera, M., Ueki, M., Watanabe, N., Takada, H., Takezaki, S., Chida, N., Kobayashi, I., Ariga, T., 2014. Two novel gain-of-function mutations of STAT1 responsible for chronic mucocutaneous candidiasis disease: impaired production of IL-17A and IL-22, and the presence of anti-IL-17F autoantibody. J. Immunol. 193, 4880–4887.

Zhong, M., Henriksen, M.A., Takeuchi, K., Schaefer, O., Liu, B., ten Hoeve, J., Ren, Z., Mao, X., Chen, X., Shuai, K., Darnell, J.E., 2005. Implications of an antiparallel dimeric structure of nonphosphorylated STAT1 for the activation-inactivation cycle. Proc. Natl. Acad. Sci. U.S.A. 102, 3966–3971.